Article

Banki-Michell Optimal Design by Computational Fluid Dynamics Testing and Hydrodynamic Analysis

Vincenzo Sammartano [1,*], **Costanza Aricò** [1], **Armando Carravetta** [2], **Oreste Fecarotta** [2] **and Tullio Tucciarelli** [1]

[1] Department of Civil, Environmental, Aerospace and Materials Engineering, University of Palermo, Viale delle Scienze edificio 8, 90128, Palermo, Italy; E-Mails: costanza.arico@unipa.it (C.A.); tullio.tucciarelli@unipa.it (T.T.)

[2] Department of Civil, Structure and Environmental Engineering, University of Naples Federico II, Via Claudio 21, 80125, Naples, Italy; E-Mails: arcarrav@unina.it (A.C.); oreste.fecarotta@unina.it (O.F.)

* Author to whom correspondence should be addressed; E-Mail: vincenzo.sammartano@unipa.it; Tel.: +39-091-238-96517; Fax: +39-091-6657749.

Abstract: In hydropower, the exploitation of small power sources requires the use of small turbines that combine efficiency and economy. Banki-Michell turbines represent a possible choice for their simplicity and for their good efficiency under variable load conditions. Several experimental and numerical tests have already been designed for examining the best geometry and optimal design of cross-flow type machines, but a theoretical framework for a sequential design of the turbine parameters, taking full advantage of recently expanded computational capabilities, is still missing. To this aim, after a review of the available criteria for Banki-Michell parameter design, a novel two-step procedure is described. In the first step, the initial and final blade angles, the outer impeller diameter and the shape of the nozzle are selected using a simple hydrodynamic analysis, based on a very strong simplification of reality. In the second step, the inner diameter, as well as the number of blades and their shape, are selected by testing single options using computational fluid dynamics (CFD) simulations, starting from the suggested literature values. Good efficiency is attained not only for the design discharge, but also for a large range of variability around the design value.

1. Introduction

The exploitation of renewable energy sources (RES) is necessary due to many contingent factors: increase in oil prices, depletion of fossil fuels and the emission limitations imposed by the Kyoto Protocol. The use of RES includes small hydroelectric power (less than 1–3 MW) located along small rivers [1,2] or along water transmission and distribution pipeline systems [3,4] and characterized by continual changes occurring in the turbine operating conditions (discharge and/or load).

Unfortunately, there is a lack of good design practice for small hydroelectric power-plants, probably because of the wide variability of the operating conditions (read variations in discharge and load, geometry of grip and release, *etc*.). Only a few authors provide guidelines [5,6] and this deficit severely limits the uptake and development of minor hydropower plants.

Banki-Michell turbines—also called cross-flows—are frequently used along small rivers. Their popularity stems from the simplicity of design and construction. An analytical approach is generally used to assess the geometry of the turbine at the best efficiency point (BEP), based on the available experimental and numerical tests. A number of rules for the choice of turbine inlet, turbine impeller and turbine chamber parameters have also been given simply based on the results of numerical simulations. On the other hand, also due to the large range of possible operating conditions, Banki-Michell devices are still far from having a standard design rule and the development of the turbine for any specific case is still pioneering.

2. The State of the Art on Michell-Banki Parameter Design

The Michell-Banki turbine is an impulse turbine optimized to work with low flows (from a few liters per second to several hundred liters per second) and low jumps (from a few meters to hundreds of meters), ranking in the turbine-discharge-load diagram near the origin of the axes. Water, coming from a river or a pipe, is conveyed toward the impeller, housed in a special production chamber by a duct element with a rectangular section. A distributor may be present to partialize the duct section according to the actual discharge value. The impeller has the shape of an empty wheel, consisting of two circular plates linked by a series of blades, shaped so that the jet is directed towards the center of the wheel and then again crossing other blades before exiting. The jet then passes through the impeller and this is the origin of the name "cross-flow". The impeller is connected to an asynchronous generator for the electricity production.

An extensive literature review on the development of hydraulic cross-flow turbines, starting from the pioneering studies of Haimerl (1960) is reported in [7–10]. Fiuzat and Akerkar [9] and De Andrade *et al.* [11] have shown that the water flow within the impeller still possesses an appreciable energy content when it reaches the blade output (the energy at the blade output is 25%–35% of the energy at the inlet blades), where there is a second energy transfer from the water flow to the turbine.

The consequence of this second transfer is that an important contribution to the overall efficiency of the machine comes from many features of the power-plant: the geometry of the supply line and the

distributor, the hydrodynamic conditions inside the impeller and at the outlet. Assuming zero pressure at the impeller outlet, Mockmore and Merryfield [12] defined the hydraulic efficiency of the machine η_{idr} as the ratio between the power available for production by the machine (P_t) and the input power P_{in} related to the hydraulic head H_{in} at the inlet of the machine, and for a given water discharge Q:

$$\eta_{idr} = \frac{P_t}{P_{in}} \cong \frac{P_t}{\rho \cdot g \cdot H_{in} \cdot Q} \tag{1}$$

where g is the gravitational acceleration and ρ is the water density.

The machine efficiency defined in Equation (1) is strongly affected by the geometry of the nozzle and the impeller. In Figure 1a vertical section and a plane view of a cross flow turbine is reported. The main impeller design parameters, shown in Figure 1, are the following: the angle α between the particle velocity and the tangent direction at the impeller inlet, the outer and inner diameters D_1 and D_2 of the impeller, the angles β_1 and β_2 of each blade with respect to the tangent direction respectively at the outer and the inner diameters, the blade number and thickness, the angle λ of the arc available for the discharge inlet along the impeller outer circumference, and the ratio W/B, where B is the nozzle width and W is the impeller width. We assume in the first step of the design that the shape of the distributor is able to guarantee an approximately constant angle α all along the outer circumference of the inlet impeller.

Figure 1. Geometrical parameters of the cross flow turbine.
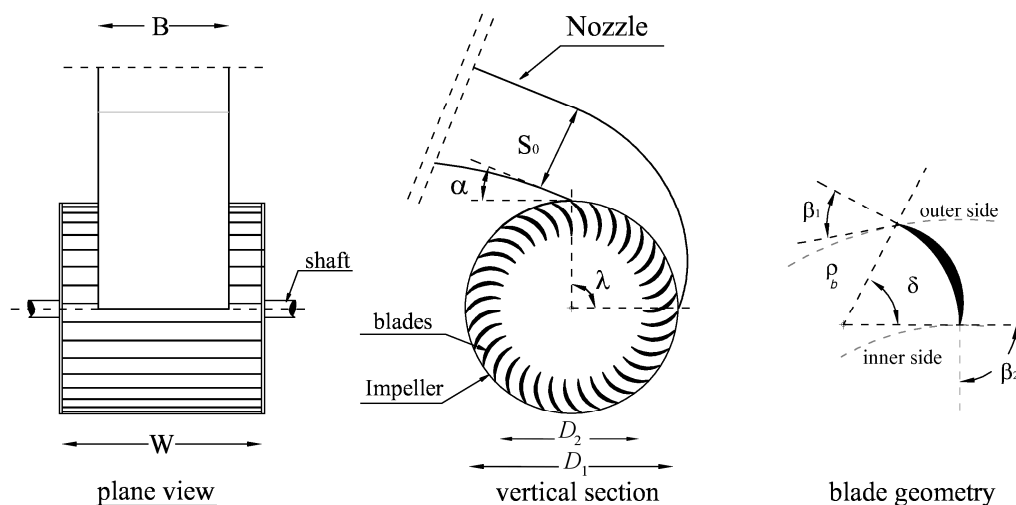
Mockmore and Merryfield suggest adopting an angle α equal to 16°, claiming that this is a good compromise between the need to maximize hydraulic and structural efficiencies [12]. Later, Fiuzat and Akerkar observed from experimental data that the maximum efficiency corresponds to an attack angle α equal to 24° [8]. In their experiments Aziz and Desai used a range of attack angle starting from 22° to 32° with steps of 2°, and observed that the maximum efficiency can be obtained with an attack angle α equal to 22° [10]. Moreover, Aziz and Totapally observed that with an angle of attack of 22° the efficiency of the turbine was about 90% [13]. Choi *et al.* investigated the effect of the turbine's geometry on performance and internal flow characteristics by using some computational fluid dynamics (CFD) simulations [14]. The results of this study highlighted that decreasing the attack

angle, from 35° to 25°, the efficiency of the turbine increases accordingly by 60% to 80%. With this noted, previous studies show that α is probably the most important design parameter and it should be set at the minimum value compatible with the structural and technological needs of the blades and the maximum size of the impeller. A 22° value is suggested by several authors [10,13].

Mockmore and Merryfield [12] suggested the following relationship between α and β_1 value:

$$tan\,\beta_1 = 2 \cdot tan\,\alpha \tag{2}$$

Relationship (2) can be motivated by the need to avoid abrupt discontinuities between particle velocity immediately inside and outside the rotating impeller. The angle β_1 that avoids any discontinuity in the path of the water particle entering the impeller is the one that satisfies the following condition:

$$\frac{1}{tan\,\beta_1} = \frac{1}{tan\,\alpha} - \frac{\omega \cdot D_1}{2 \cdot V_r} \tag{3}$$

where V_r is the radial component of the particle velocity V and ω is the angular velocity of the rotating reference system. We will show in the following section that Equation (3) is equivalent to Equation (2) when the velocity of the rotating system is half of the component of the particle velocity in the tangent direction.

Many researchers agree that the optimum value of β_2 is $\pi/2$ [10–13]. This value provides a radial direction to the relative outlet velocity inside the impeller at the inner diameter (D_2), and this leaves to the fluid, in the inner part of the impeller, only the energy of the rotating system, which can be recovered during the next blade crossing. Mockmore and Marryfield [12] derived the expression of the maximum efficiency according to some restrictive hypotheses and to Relationship (3), as a function of the angle α:

$$\eta_{max} = \frac{C^2 \cdot (1+\psi) \cdot cos^2\,\alpha}{2} \tag{4}$$

where C and Ψ are reduction parameters (proposed equal to 0.98), depending respectively on the nozzle and on the impeller geometry.

An increment in the diameter ratio (D_2/D_1) corresponds to a stronger curvature of the impeller blades, because the blade angle has to shift from the β_2 to the β_1 value in a shorter distance. This implies stronger turbulence, but also a shorter distance for energy transfers. Aziz and Totapally suggest that the maximum efficiency is achieved with a diameter ratio of 0.68 [13].

The effect of the number of blades N_b on turbine efficiency has been explored by experimental and numerical studies [13–17]. The studies showed that an increment in the blade number has a positive impact on the efficiency of the turbine, due to a more regular velocity profile inside the space between each couple of blades. In particular, Aziz and Totapally observed that an increment in efficiency can be obtained by increasing the number of blades from 15 to 35 [13]. On the other hand, a further increase provides larger energy dissipation due to a strong effect of the blades solid walls. Choi *et al.*, using CFD analyses, observed the same trend as Aziz, but the maximum efficiency of the turbine was obtained in the case of an impeller with 30 blades [14].

Aziz and Desai [10] and Nakase *et al.* [18] carried out a series of experiments by which they observed that the flow stream spread W/B can have a positive effect on turbine performance, with an increment in efficiency, up to a spread value W/B of 1.5. The reason is that the normal section of the

flow rate entering the impeller from the blades is subject in the radial direction of the plane normal to the turbine axis to: (1) a restriction due to the radial convergence of the particle trajectories; (2) an extension due to the centrifugal forces. When these two effects do not balance each other, an extension of the flow section in the axis direction is possible. In this case, the 3D behavior of the velocity field is important, as well as the corresponding numerical modeling. Experimental studies [8,9,18] showed that the inlet discharge angle (λ) influences cross-flow efficiency. For a given flow rate, a smaller arc corresponds to higher inlet velocities, but also to a smaller divergence of the particle paths after entering the impeller from the blades. The authors of the mentioned papers [8,9,18] observed that a nozzle with $\lambda = 90°$ is more efficient than a nozzle with $\lambda = 120°$. It is important to optimize the shape of the distributor in order to obtain an almost constant α angle along the impeller outer circumference. This optimization allows one to limit the variation of the velocity directions close to the blades' surfaces. De Andrade *et al.* have shown through experiments that for a fluid draft entry angle of $\alpha = 16°$, the actual input angles vary between 7° and 23° [11]. Lastly, to ensure stable flow conditions within the impeller, it is important to provide the production chamber with one or more air inlets, in order to adjust the depression which arises in the chamber as a result of air entrainment by the jet. Choi *et al.* have shown through numerical experiments that increased air supply can increase the efficiency of the turbine, and explained this result with a better flow exit angle from the impeller [14].

The previous results are summarized in Table 1.

Table 1. Design parameters according to previous studies.

Design parameters	values	Description of the design parameters
D_2/D_1	0.68	Diameter Ratio
α	22°	Angle of attack
β_2	90°	Blade exit angle
λ	90°	Inlet discharge angle
N_b	35	Number of blades

3. The Proposed Two-Step Design Procedure

The referenced studies on the design of the Banki-Michell turbine were heavily based on laboratory tests and, more recently, on numerical simulations of single cases, but a theoretical framework for a fast sequential design of the turbine parameters is still missing.

In the present paper a standard procedure is proposed for the design of a Banki-Michell turbine, based on two different steps. The first step is the design of the outer diameter of the impeller D_1 and of the blade attack angle β_1, for given water discharge Q and hydraulic head H, as well as of the nozzle profile. The maximum efficiency attainable in these conditions is derived from the Euler's equation for rotating machines and from the assumption of zero energy dissipation inside the nozzle. The other impeller parameters are estimated by testing single options by means of CFD analysis. The inner diameter D_2 is optimized by evaluating the efficiency of the turbine for different values of the diameter ratio D_2/D_1; the inner radius blade, the attack angle, the number of blades, their shape and the inner/outer diameter ratio are optimized starting from known literature results. Computations can be carried out in cases both of zero downstream pressure (where the air phase is present in the impeller case) and non-zero downstream pressure (where the impeller case is fully pressurized).

The power P_t transferred from the current flow to the rotating system, according to the Euler's equation can be written in the following form:

$$P_t = \rho \cdot Q \cdot \left[\left(\vec{V_1} \cdot \vec{U_1} - \vec{V_2} \cdot \vec{U_2} \right) + \left(\vec{V_3} \cdot \vec{U_3} - \vec{V_4} \cdot \vec{U_4} \right) \right] \tag{5}$$

where $\vec{V}$ is the particle velocity, $\vec{U}$ is the velocity of the rotating reference system and Q is the water discharge (see Figure 2). The underlying assumption is that there is a radial symmetry of the velocities along all the inlet and outlet arc of both the inner and outer impeller circumferences. This is, of course, a simplification of reality. The particles with low inlet velocity could not even enter the impeller, due to the centrifugal forces (as mentioned in [13]).

Figure 2. Points in the Euler's equation.
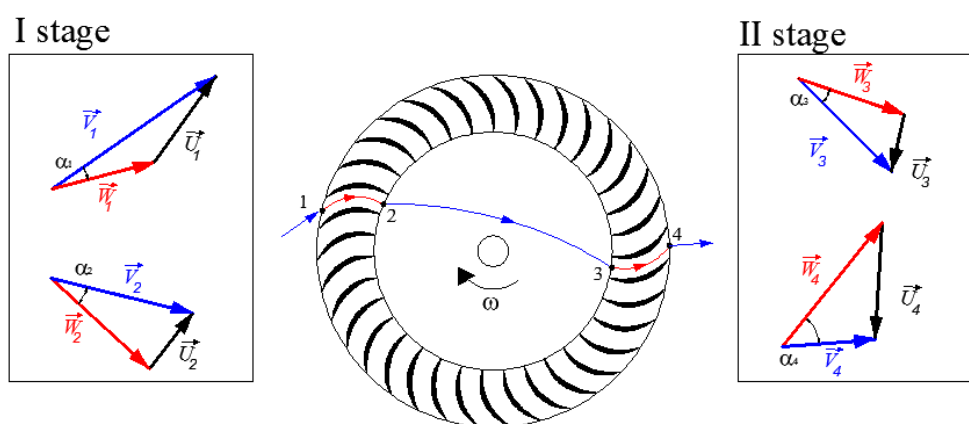
The power in Equation (5) has four components, which we call P_1, P_2, P_3 and P_4. Assuming a β_2 blade angle equal to $\pi/2$, the sum of the second and third components is equal to:

$$P_2 + P_3 = \rho \cdot Q \cdot \left(-U_2^2 + U_3^2 \right) = 0 \tag{5b}$$

because on the blade surface the component of the particle velocity in the direction of the reference system velocity is equal to the norm of the same velocity ($U_2 = U_3$).

If a further assumption is made by neglecting the fourth power component P_4, and assuming that almost all the fluid energy has been either transferred or dissipated before leaving the impeller, the only component affecting the turbine efficiency remains the first one. Thus, Equation (5) could be simplified and becomes:

$$P_t \cong \rho \cdot Q \cdot \left(\vec{V_1} \cdot \vec{U_1} \right) \tag{6}$$

Equation (6) holds if the norm V at point 1 (see Figure 2) is the same immediately inside and outside the impeller and the velocity continuity must also hold around the blade surface. Because a simplifying assumption is made that the velocity has radial symmetry at the impeller inlet, Equation (6) only holds if the norm U of the velocity of the reference system is equal to the component of the particle velocity $\vec{V}$ in the tangent direction minus the tangential component of the relative velocity $\vec{W}$ (see Figure 2). This implies the equality:

$$U_1 = V_1 \cos \alpha - W_{1,t} \tag{7}$$

where $W_{1,t}$ is the tangential component of the relative velocity $\vec{W}$. Thus, Equation (6) can be written as:

$$P_t = \rho \cdot Q \cdot V_1 \cos \alpha \cdot \left(V_1 \cos \alpha - W_{1,t} \right) \tag{8}$$

All the energy of the entering flow can be either dissipated or transferred to the rotating system if:

$$W_{1,t} = \frac{V_1 \cos \alpha}{2} \tag{9}$$

and, in the ideal case of $\cos \alpha = 1$,

$$W_{1,t} = \frac{V_1}{2} \tag{9b}$$

Moreover, if we assume that the relative velocity $\vec{W}$ satisfies Equation (9), we can see from Equation (8) that the efficiency η of the turbine has an upper theoretical limit, given by the constraint:

$$\eta \leq \cos^2 \alpha \tag{10}$$

as already found by Mockmore and Merryfield [12] with a different procedure.

3.1. First Step: Design of Basic Parameters

Equations (4) and (10), even if obtained from a strong simplification of reality, highlight why the inlet velocity angle α is such an important design parameter. On the other hand, we will show in the following sections that its choice has a strong impact on the inlet width B and on the resulting structural stress.

Let us assume the water discharge Q, the hydraulic head H and the angular velocity ω to be input data of the problem and the design inlet discharge angle λ to be taken from the literature experience. If we assume the optimal value of the relative tangent velocity to maintain the value computed in Equation (9), we can compute either the diameter D_1 or the α angle by substituting Equation (9) in Equation (7). Assuming that $U = \omega \, D_1 / 2$, we obtain:

$$\frac{V \cos \alpha}{2} = \omega \cdot \frac{D_1}{2} \tag{11}$$

Equation (11) allows one to compute either the outer diameter D_1 starting from the α angle, or vice versa. Once both D_1 and the inlet velocity angle α are known, the blade β_1 angle can be computed as the inverse of the tangent function, equal to the ratio between the velocity relative components, that is:

$$\beta_1 = \arctan \frac{V \sin \alpha}{V \cos \alpha - \omega \cdot D_1 / 2} \tag{12}$$

Observe that, when the angular velocity of the reference system (ω) is equal to half the velocity component in the tangent direction and condition (9) is attained, the same optimal relationship between α and β as suggested by Mockmore and Merryfield [12], and already mentioned in Equation (2), is found.

The main nozzle parameters are the following: the nozzle initial height S_0, its width B and the shape of the wall between its tip and the initial rectangular section with height S_0 (see Figure 1). The height

S_0 is a function of the specific water discharge q (per unit width), and this can be directly computed according to the continuity equation applied at the inlet of the impeller:

$$q = V \sin\alpha \cdot \lambda \cdot \frac{D_1}{2} \qquad (13)$$

Mass conservation requires (see Figure 1):

$$\begin{cases} S_0 = \dfrac{q}{V} \\ B = \dfrac{Q}{q} \end{cases} \qquad (14)$$

The lower (plane) wall of the initial nozzle forms an angle α with the tangent direction in the initial point of the impeller inlet arc. The same angle α is formed by the direction of the upper wall with the tangent direction at the tip of the nozzle.

It is observed that the specific discharge q is proportional to *sin α* (see Equation (13)) and that the impeller width B is inversely proportional to q (see Equation (14)). The choice of the angle α and the outer diameter D_1 stems mainly from a balance between the search of a low angle α (and a high hydraulic efficiency according to Equation (10)) and the need to limit the width B of the nozzle resulting from Equation (14), because the blade length W (W > B) strongly affects the mechanical stress inside the same blades. Moreover, by reducing the angle α, the ratio between the free inlet surface of the impeller and the total inlet surface of the same impeller drops due to the enhanced effect of the blade thickness.

The shape of the upper wall has been defined by adopting a linear relationship between the radius of curvature r and the angle θ, that is the angle between the radial and the horizontal directions, as shown in Figure 3a. The linear variation of the upper wall of the nozzle is aimed to get an approximately constant angle α along the impeller inlet. The reason is that, assuming a constant angle α and a constant velocity norm V (that is to say neglecting energy dissipation) with such an upper wall profile, mass continuity is globally satisfied in each partial volume where the entering flux surface is proportional to the remaining arc length (see Figure 3b). In each partial volume depicted in Figure 3b, neglecting the transition zone between the no-slip velocity at the upper wall and the fully developed internal velocity, the entering and the leaving fluxes (q_e and q_l respectively) are equal to:

$$q_e = V \cdot S_0 \frac{\theta}{\lambda} \qquad (15a)$$

$$q_l = q_e = (V \sin\alpha) \cdot \frac{D_1}{2} \cdot \theta = V_r \cdot \frac{D_1}{2} \cdot \theta \qquad (15b)$$

where $V_r \cdot$ is the radial velocity. According to this hypothesis the upper wall radius $r(\theta)$ is equal to:

$$r(\theta) = K \cdot \theta + \frac{D_1}{2} \qquad (16)$$

where K is a constant. The radius r at the nozzle initial height S_o can be calculated as:

$$r_{(\lambda-\gamma)} = \frac{S_0 \cos\alpha + \dfrac{D_1}{2}}{\cos\gamma} \tag{17}$$

Figure 3. Nozzle upper wall shape: (**a**) geometric scheme; (**b**) entering and leaving water flow in the nozzle.
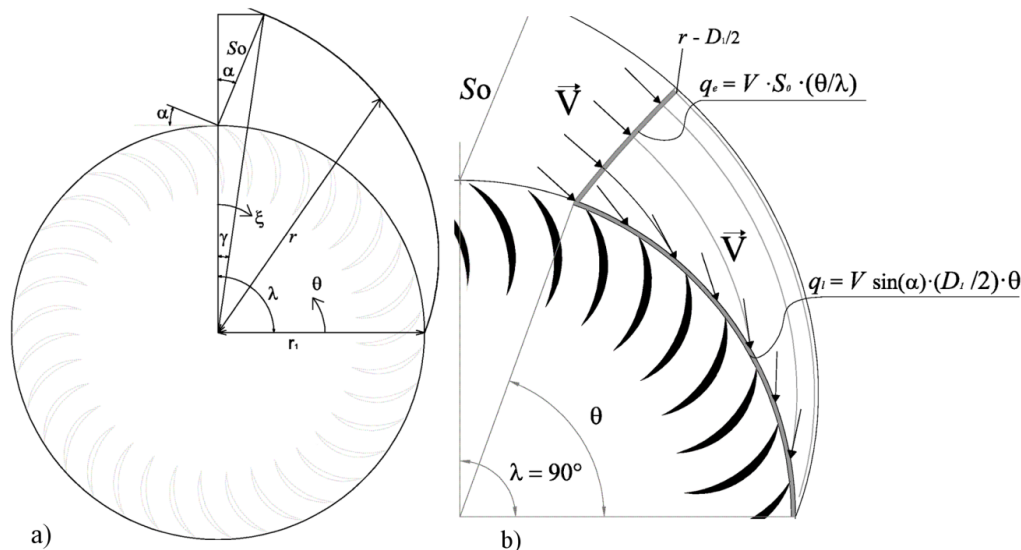
where

$$\gamma = arctg \frac{S_0 sen\alpha}{S_0 \cos\alpha + \dfrac{D_1}{2}} \tag{18}$$

Equations (17) and (18) make it possible to calculate the constant K in Equation (16), as:

$$K = \frac{1}{\lambda-\gamma} \left[\frac{S_0 \cos\alpha + \dfrac{D_1}{2}}{\cos\gamma} - \frac{D_1}{2} \right] \tag{19}$$

The hypothesis of a homogeneous attack angle along the impeller inlet will be further validated with reference to a specific case.

3.2. Second Step: Impeller Parameters Optimization

The variation in the diameter ratio D_2/D_1 affects the efficiency of the cross-flow turbine: an increment of the diameter ratio leads to a reduction in the blade radius, a reduction of the blade surfaces and a shorter distance for energy transfers. In order to select the optimal internal diameter D_2, a sensitivity analysis on the diameter ratio can be carried out by using a fluid dynamic investigation. As will be shown in the methodology testing, the sensitivity analysis often leads to a diameter ratio very close to the 0.68 literature value.

After the diameter ratio has been chosen, the geometry of the inner blade surface can easily be calculated. For simplicity, this surface is designed as part of a cylinder, whose axis is located at the intersection of the two directions orthogonal to the relative velocities at the inlet and at the outlet, as shown in Figure 4. The exit angle β_2 is set equal to 90° and the blade radius ρ_b and the central angle δ can be computed as follows:

$$\begin{cases} \rho_b = \dfrac{D_1}{4} \cdot \left[1 - \left(\dfrac{D_2}{D_1} \right)^2 \right] cos(\beta_1)^{-1} \\ tan\left(\dfrac{\delta}{2} \right) = \dfrac{cos(\beta_1)}{sin(\beta_1)} \end{cases} \tag{20}$$

Figure 4. Blade geometry.
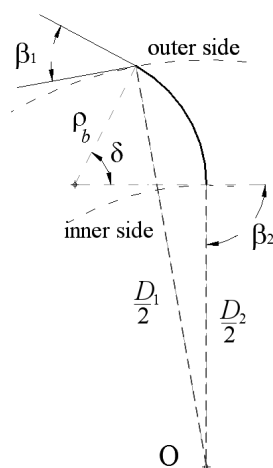
Other impeller parameters are the inlet angle, the shaft diameter, the number of blades and their thickness as function of the radius *r*. All these parameters must be selected according to a numerical fluid and structural dynamic investigation. In order to obtain an impeller with the maximum efficiency, the width of the impeller B was initially set larger than the nozzle width W, W/B = 1.5, in agreement with some previous studies [10,18].

4. Fluid Dynamic Investigation by CFX Code

Fluid dynamic calculations were performed for a specific case to show the practical implementation of the design strategy outlined in the previous two-step procedure. A first series of simulations were carried out by using a quasi 2D model, in order to reduce the computational time. Because the implemented software (ANSYS-CFX) does not allow two-dimensional fluid dynamic simulations [19], the 2D problem was solved by generating a mesh extruded to a single layer and by imposing symmetry on the two side faces. A second series of 3D numerical simulations was carried out in order to verify whether the flow stream spread W/B has a positive effect on turbine performance. In the two series of simulations the computational domain was divided using both tetrahedral and prismatic elements. The prismatic elements were used to discretize the computational domain inside the near-wall region along the blades and the boundary surfaces, where a boundary layer is present, while the tetrahedral elements

were used to discretize the remaining domain. The algorithm used in CFX to create the tetrahedral element discretization is called "Patch Conforming", that is a Delaunay tetra mesher with an advancing-front point insertion technique used for mesh refinement [19]. The prismatic elements were created by using the "Pre Inflation" algorithm, so the surface mesh would be inflated first, and then the rest of the volume mesh could be generated [19]. In Figure 5, an example of the mesh used for the 2D simulation series is shown: in this configuration the two physical domains of the stator (nozzle and casing) and the rotor were divided into 35,801 and 65,422 finite volumes, respectively.

Figure 5. 2D-computational mesh with a zoom view close to the inlet of the impeller.
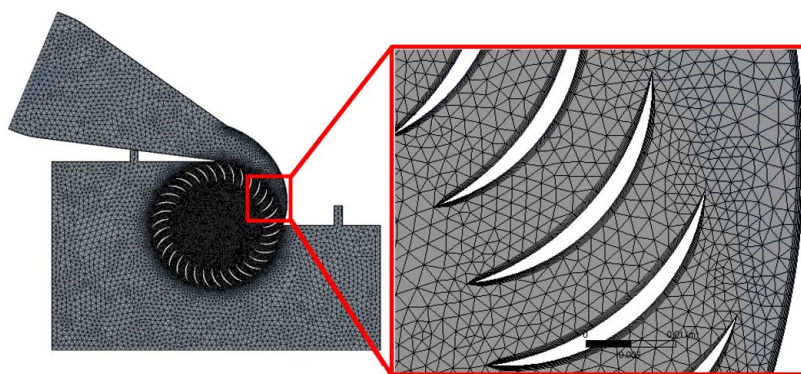
In the second set of simulations, the 3D domain is still divided into two sub-domains, rotor and stator. As shown in Figure 6, the 3D domain was divided into two symmetric parts, but only one was modeled and solved, assuming an impermeable boundary along the symmetry plane. The computational domain was discretized with tetrahedral elements and, close to the boundary surfaces, with prismatic elements in order to capture the strong gradients of the physical/cinematic flow variables. In this way the stator and the rotor domains were divided into 679,605 and 2,667,986 finite volumes, respectively. These choices allowed a strong reduction in the computational time. The quality of the mesh was verified by using a pre-processing procedure by ANSYS® ICEM CFD™ [19].

Figure 6. 3D-computational mesh with a zoom view close to the inlet of the impeller (case with W > B).
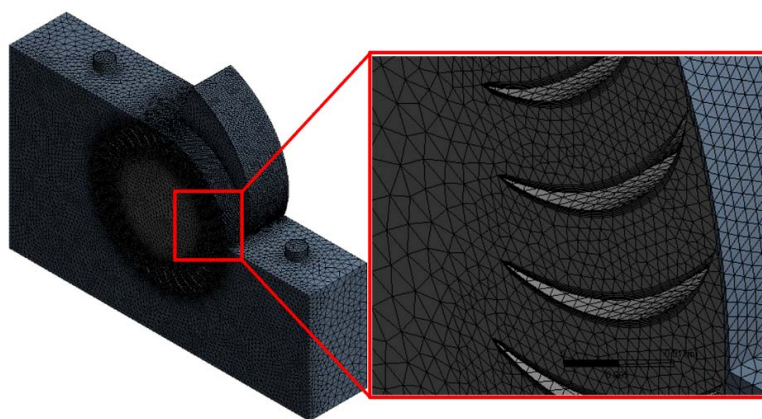
Both water and air phases were modeled in the computational domain according to the free surface homogeneous model [19]: according to this model the two fluids share the same dynamic fields of

pressure, velocity and turbulence. In homogeneous multiphase flow, two phases coexist: water (*w*) and air (*a*). This is denoted as α_l, ρ_l, μ_l and U_l; respectively, the volume fraction, the density, the viscosity and the mean in time value of velocity vector for phase *l* (*l* = *w*, *a*), that is:

$$\rho = \sum_{l=w,a} \alpha_l \rho_l \tag{21.a}$$

$$\mu = \sum_{l=w,a} \alpha_l \mu_l \tag{21.b}$$

where ρ and μ are the density and the viscosity of the "averaged" phase. The air density is assumed to be function of the pressure *p*, according to the state equation:

$$\rho_a = \rho_{a,0} e^{\gamma(p-p_o)} \tag{21.c}$$

where the sub-index 0 marks the reference state values and γ is the air compressibility coefficient.

The governing equations are: (1) the mass conservation equation; (2) the Reynolds averaged continuity equation of each phase; and (3) the Reynolds averaged momentum equations. Mass conservation implies:

$$\sum_{l=w,a} \alpha_l = 1 \tag{22}$$

The Reynolds averaged continuity equation of each phase can written as:

$$\frac{\partial \rho_i}{\partial t} + \nabla \cdot (\rho_i \mathbf{U}) = S_i \tag{23}$$

where S_i is an external source term. The momentum equation is instead referred to the "averaged" phase:

$$\frac{\partial (\rho \mathbf{U})}{\partial t} + \nabla \cdot (\rho \mathbf{U} \otimes \mathbf{U}) - \nabla \cdot \left(\mu_{eff} \left(\nabla \mathbf{U} + (\nabla \mathbf{U})^T \right) \right) + \nabla p' = S_M \tag{24}$$

where $\otimes$ is the dyadic symbol; S_M is the momentum of the external source term S; μ_{eff} is the effective viscosity accounting for turbulence and defined as:

$$\mu_{eff} = \mu + \mu_t \tag{25}$$

where μ_t is the turbulence viscosity and p' is the modified pressure, equal to:

$$p' = p + \frac{2}{3} \rho k + \frac{2}{3} \mu_{eff} \nabla \cdot \mathbf{U} \tag{26}$$

where k is the turbulence kinetic energy, defined as the variance of the velocity fluctuations; and p is the pressure. All the phases share the same pressure p and the same velocity $\mathbf{U}$. To close the set of six governing scalar equations [Equations (22) and (23) (two) and Equation (24) (three)], a $k-\varepsilon$ turbulence model is applied. The unknowns of the problem are: (1) pressure p; (2) the scalar components U_i (*i* = 1, 2, 3 of the velocity field); and (3) the volume fraction of each phase (two). The computational domain is divided into two sub-domains: the stator (nozzle and casing) has an inertial reference system; the rotor (impeller) has a non-inertial reference system, integral with the rotation axes of the rotor. In the CFX code, the interface model "general connection" was set, since the reference system changes at the interface of the abovementioned sub-domains. The "transient

rotor-stator" option was also selected to take into account the transient effects along the abovementioned interface. Using this option, the interface position was updated at each time step, and the relative position of the grids on each side of the interface changes. At the entrance of the nozzle volume fractions were set at zero for air and one for water. At the base of the production chamber, at the water outlet, a pressure value of 1 atm was imposed as a boundary condition, enabling the possible flow of air from the outside towards the inside of the machine. The same boundary condition was imposed in the nodes along the air vents.

5. Impeller Design Testing

As already stated in the previous section, two series of simulation were performed: 2D simulations were carried out to define the optimum geometry of the impeller with the exception of the optimal W/B ratio, while 3D simulations were carried to investigate the optimal value of the spread ratio W/B. For each series of numerical computations the same project input data was used: water discharge Q equal to 60 l/s, angular velocity ω equal to 757 rpm, input velocity norm V equal to 13.7 m/s. The outflow boundary condition is set equal to zero relative pressure. The cross flow turbine is assumed to be an action machine. According to this assumption, the computed relative pressure at the nozzle inlet should be zero. If this was not the case, the resulting inlet total head would be equal to the kinetic energy corresponding to V, plus the computed piezometric depth. The attack angle α, the outer diameter of the impeller D_1, parameters B, β_1 and the profile of the nozzle external wall (parameters S_o and K) were computed according to Equations (11)–(19) reported in step 1 of the procedure. The geometry of the impeller blades (ρ_b and δ) was computed according to Equation (20), reported in step 2 of the procedure, assuming a diameter ratio D_2/D_1 equal to 0.68, as suggested in the literature [8,13,18]. It was also assumed that a value $\alpha = 22°$ provides the best equilibrium between hydraulic efficiency and mechanical strength, as also suggested in the literature [10,13]. The other parameters were initially set equal to the values suggested in the literature. The geometry of the resulting cross flow turbine is reported in Table 2.

Table 2. Geometrical parameters of the impeller.

Parameter	value	Description of the geometrical parameters
D_1 (mm)	161	Impeller outer perimeter diameter
D_2 (mm)	109	Impeller inner perimeter diameter
N_b (-)	35	Number of blades
λ (°)	90	Inlet discharge angle
α (°)	22	Attack angle of the outlet nozzle velocity
β_1 (°)	38.9	Angle between the blade and the outer perimeter of the impeller
β_2 (°)	90.0	Angle between the blade and the inner perimeter of the impeller
ρ_b (mm)	27.7	Radius of blade
δ (°)	61.5	Central angle of blade
S_0 (mm)	47	Nozzle initial height
B (mm)	93	Nozzle width
K (-)	31.5	Constant in Equation (19)
W (mm)	139	Impeller width

5.1. 2D-Simulations: Optimum Geometry Tests

Through this series of simulations the optimum geometry of the cross flow was refined. The first set of numerical simulations was conducted to verify how the number of blades affects impeller efficiency, neglecting the effect of the nozzle shape and assuming a known velocity with norm *V* and attack angle *α* equal to 22° along the outlet border of the nozzle. These simulations were carried out taking into account two physical domains: the rotor (impeller) and the stator, formed only by the casing of the turbine. The discretization of the fluid domain, the boundary and the initial conditions of this set of numerical simulations is described in section 4. The rotor and stator domains, made of tetrahedral and prismatic elements, were divided into 64,757 and 19,844 finite volumes, respectively. One of the meshes used for these simulations is reported in Figure 7.

Figure 7. Mesh of the physical domains for the simulation with a 35 blade impeller.
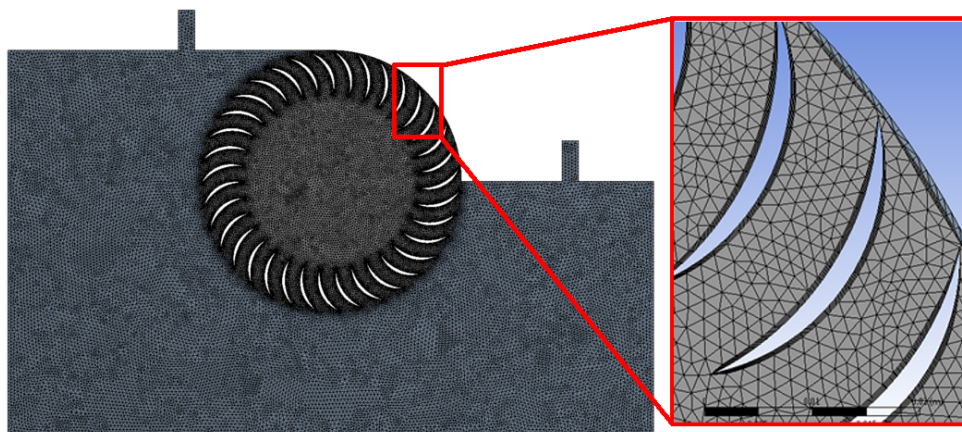
Three impellers with a different number of blades N_b equal to 30, 35 and 40 were investigated. For each simulation, the efficiency of the cross-flow turbine was calculated as the ratio between the power supplied to the impeller (applied torque *T* times the impeller angular velocity *ω*) and the power lost by water passing through the turbine (difference between the hydraulic power of the water flow in the inlet and in the outlet of the turbine):

$$\eta = \frac{T \cdot \omega}{\left(P_{inlet} - P_{outlet} \right)} \tag{27a}$$

where P_{inlet} and P_{outlet} are the hydraulic power of the water flow in the inlet and in the outlet of the turbine:

$$\begin{cases} P_{inlet} = \gamma \cdot \int_{Ainlet} H \cdot V \cdot dA \\ P_{outlet} = \gamma \cdot \int_{Aoutlet} H \cdot V \cdot dA \end{cases} \tag{27b}$$

The simulation was carried out until steady state conditions were reached (corresponding to a simulation time $T_s = 1.5$ s). In the simulation, a time step size ΔT of 0.001 sec was selected. In Figure 8 the time series of the instantaneous output power (P_{out}) corresponding to the three abovementioned configurations are shown. The efficiency displays regular oscillations, decreasing along with the number of blades N_b. The time averaged value of the output power P_{out} is equal to

5.12 KW for 30 blades (Figure 8a), 5.20 KW for 35 blades and 5.07 KW for 40 blades, while the averaged efficiency for the impeller with 30, 35 and 40 blades is, respectively, 87%, 88.4% and 86%. The optimum configuration was the impeller with 35 blades, in agreement with the experimental investigations in [13].

Figure 8. Time series of the output power P_{out} for the impeller with a different number of blades: (**a**) 30 blades; (**b**) 35 blades; and (**c**) 40 blades. The red dotted lines represent the time averaged value of the output power P_{out}.
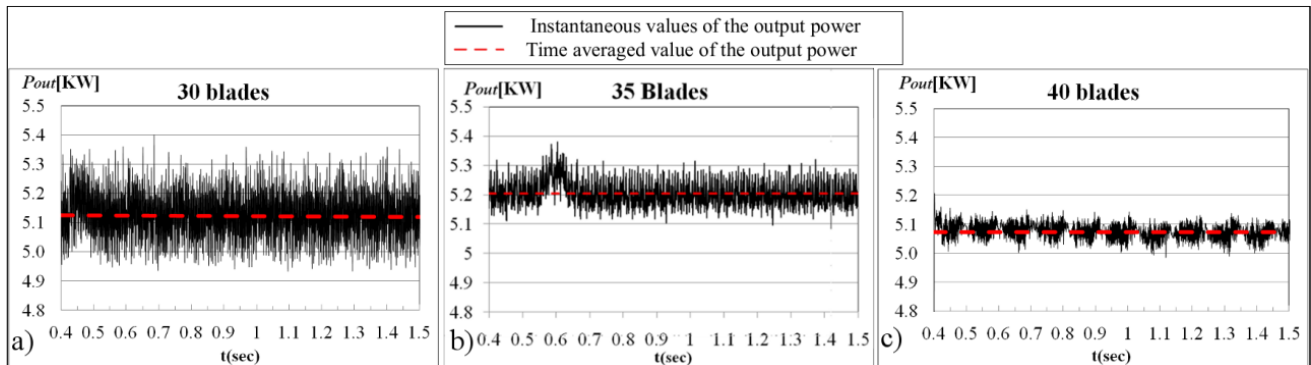
Assuming the number of blades $N_b = 35$, a numeric simulation was carried out in order to test the efficiency of the impeller with the nozzle designed by using Equations (16–19). To this aim the velocity norm *V* and the attack angle *α* along all the inlet of the impeller were computed by removing the idealized boundary condition assigned in the previous tests and solving the problem along the entire computational domain presented in Section 4. This simulation was performed taking into account two physical domains—rotor and stator—as also described in Section 4, with a total simulation time T_s of 1.5 s. For each time step the value of the turbine efficiency *η* was estimated by using Equations (27a–27b). The plot of the instantaneous output power P_{out} *versus* time is reported in Figure 9 and this shows that the output power is about 5.02 KW. The time averaged value of the efficiency *η* drops slightly to a value of 85.39%, with a limited 3.01% reduction.

Figure 9. The time series of the output power P_{out} for the turbine with 35 blades and the designed nozzle. The black dotted line represents the time averaged value of the output power P_{out} .
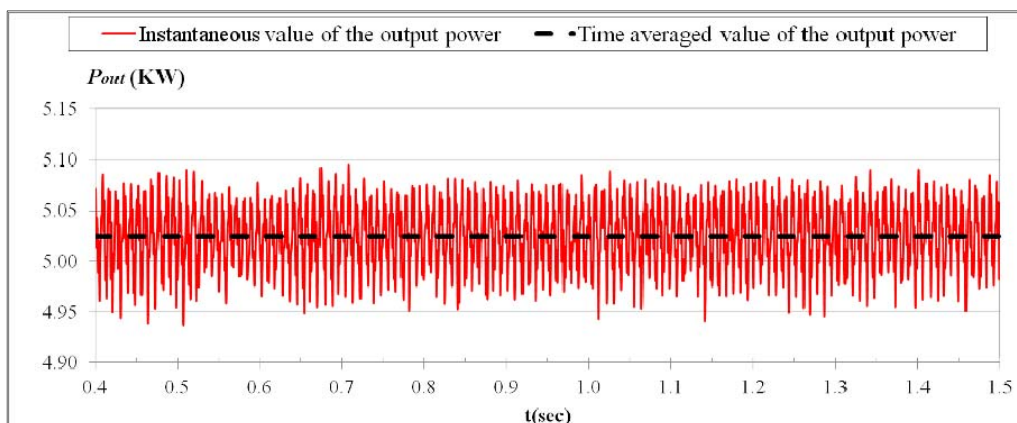
It should be observed for the final step of the simulation that: (T_s = 1.5 sec), the tangential velocity V_t ($V\cos\alpha$), the radial velocity V_r ($V\sin\alpha$) and the attack angle α evaluated at the middle points between two consecutive blades along all the inlet arc of the impeller (ξ), respectively, as shown in Figure 10 (V_t and V_r) and in Figure 11 (*a*). The average value of V_t was about 14 m/s, the average value of V_r was about 5 m/s and both remained almost constant along ξ. The attack angle α has an average value of about 21°, very close to the optimal α value suggested in the literature and adopted in the design procedure (step 1 and step 2). Moreover in Figure 12, it can be seen that the velocity norm V did not change significantly inside the nozzle. This validates the hypothesis of negligible energy dissipation.

Figure 10. The tangential velocity V_t and the radial velocity V_r at the impeller's inlet.
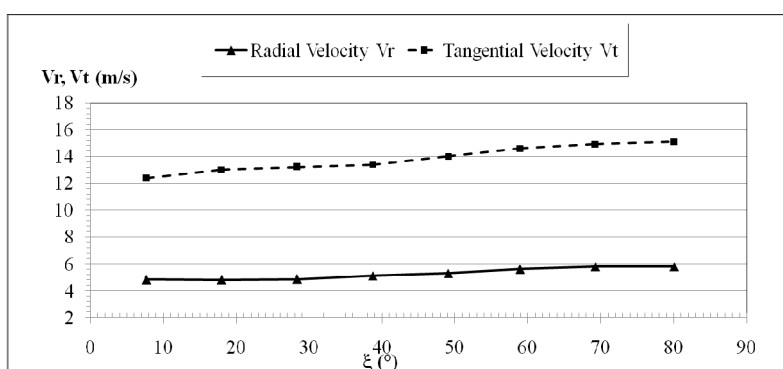
Figure 11. The attack angle α at the impeller's inlet.
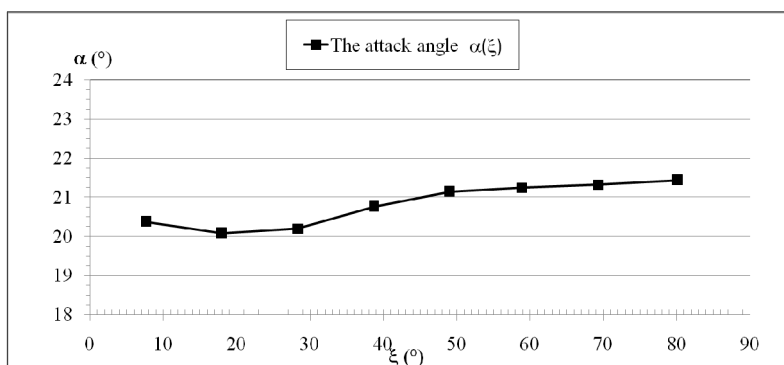
Figure 12. The average value of the velocity norm V inside the nozzle.
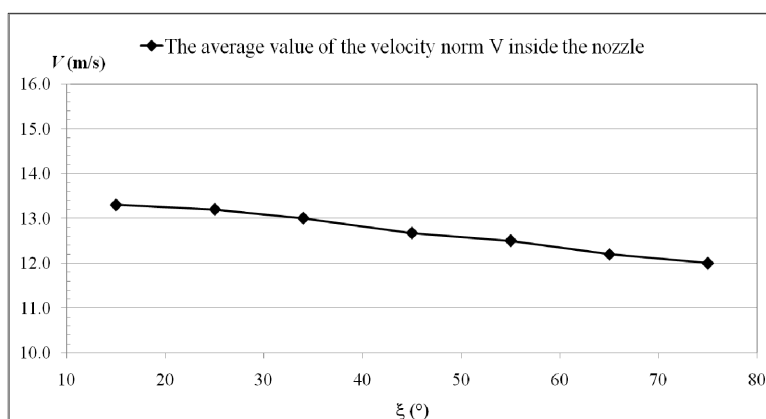
The optimal inner/outer diameter ratio was then investigated in the range 0.58 ÷ 0.78. The different tested values of the ratio D_2/D_1 and the corresponding values of the blade radius ρ_b and of the central angle δ are shown in Table 3.

Table 3. The selected diameter ratio D_2/D_1 for the sensitivity analysis.

D_2/D_1	ρ_b (mm)	δ (degree)
0.58	34	66
0.63	31	63
0.65	30	63
0.68	28	61
0.73	24	60
0.78	20	58

The impellers analyzed in the set of simulations had 35 blades and the nozzle external wall was designed according to Equations (11–19). The mesh of the physical domains, the boundary and initial conditions of the numeric simulations are the same described in paragraph 4. The duration of each simulation was 1.5 seconds with a time step of 0.001 sec. The time averaged efficiency η_a for the proposed tests is reported in Figure 13. It can be observed that the best efficiency was obtained for a diameter ratio $D_2/D_1 = 0.65$, close to the value $D_2/D_1 = 0.68$ suggested in the literature [8,13,18]. The efficiency η_a of the cross flow turbine, obtained by selecting a ratio $D_2/D_1 = 0.65$, is 85.6%.

A preliminary sensitivity analysis, for the choice of the time step value, was previously performed. Numerical simulations were carried out assuming a Δt equal to 0.0002 s. According to the output results, the computed variables (pressures, velocities) were very similar to the ones computed with Δt equal to 0.001 sec. Most importantly, the time averaged efficiencies of the two impeller configurations ($D_2/D_1 = 0.65−0.68$) did not significantly change.

Figure 13. The efficiency η_a as a function of the ratio D_2/D_1.
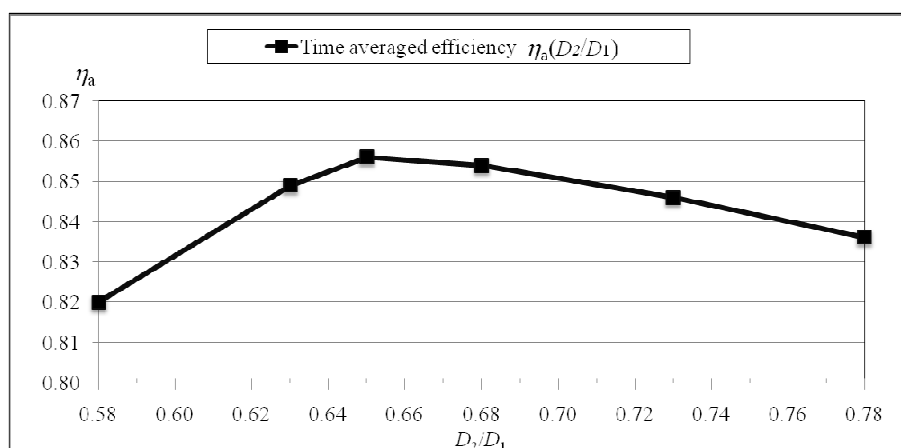
It should be noted in Figure 14 that the angle α computed along the inlet arch showed the same trend for each of the analyzed diameter ratios and was very close to the 22° project value.

The previous set of 2D computational fluid dynamic analyses made it possible to define the optimum geometry of the cross flow turbine. In Table 4 the list with all the optimum parameters of the

designed turbine is shown. The efficiency curve of this turbine was estimated using the same tool in order to verify its performance with different values of the ratio V_t/U. The efficiency curve of the turbine, reported in Figure 15, shows that the peak of efficiency was in the range $1.8 \div 2.0$. This result is in agreement with the assumption represented by Equation (11). Moreover, the average efficiency of the turbine was greater than 80% for a value of V_t/U varying between 1.2 and 3.0 (corresponding to a water discharge varying between 35 l/s and 90 l/s). In Figures 16–18 the distributions of the water volume fraction, the velocity field, and the pressure in the simulated sub-domains for the optimum configuration are shown.

Figure 14. The angle of attack α at the impeller's inlet for different values of the ratio D_2/D_1.
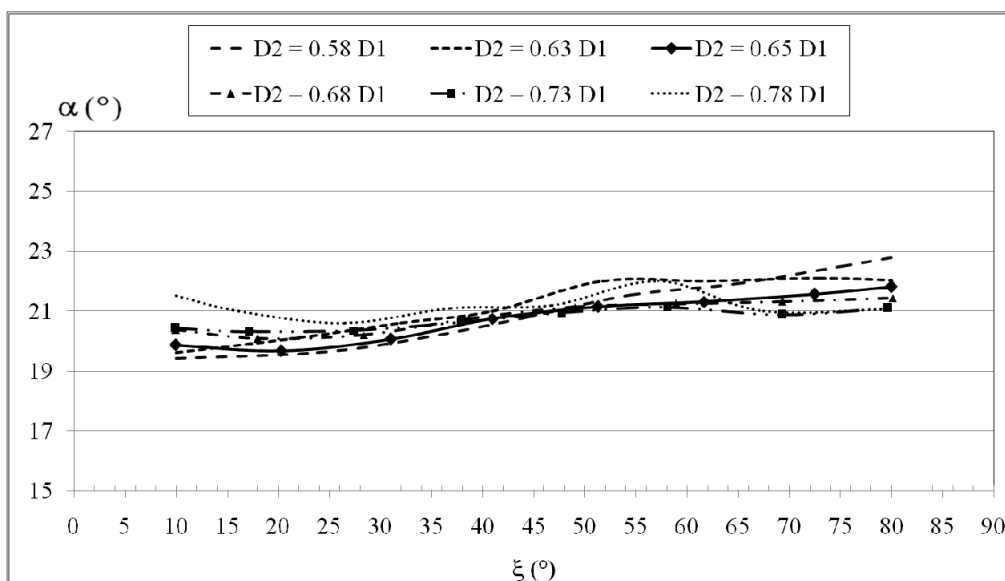
Table 4. Optimum geometry of the cross flow turbine.

Parameter	Value	Description of the geometrical parameters
D_1 (mm)	161	Impeller outer perimeter diameter
D_2 (mm)	104	Impeller inner perimeter diameter
N_b (-)	35	Number of blades
λ (°)	90	Inlet discharge angle
α (°)	22	Angle of attack
β_1 (°)	38.9	Angle between the blade and the outer perimeter of the impeller
β_2 (°)	90.0	Angle between the blade and the inner perimeter of the impeller
ρ_b (mm)	29.8	Radius of blade
δ (°)	62.6	Central angle of blade
S_0 (mm)	47	The nozzle initial height
B (mm)	93	Nozzle width
K (-)	31.5	Constant in Equation (16)
W(mm)	139	Impeller width (using W/B = 1.5)

Figure 15. Efficiency curve of the designed turbine.
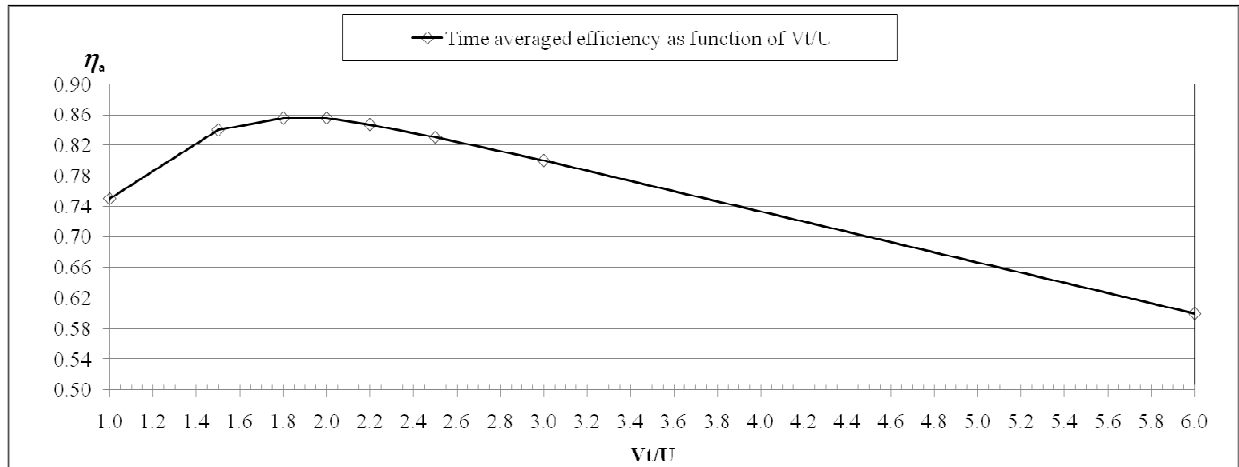
Figure 16. Water volume fraction contours.
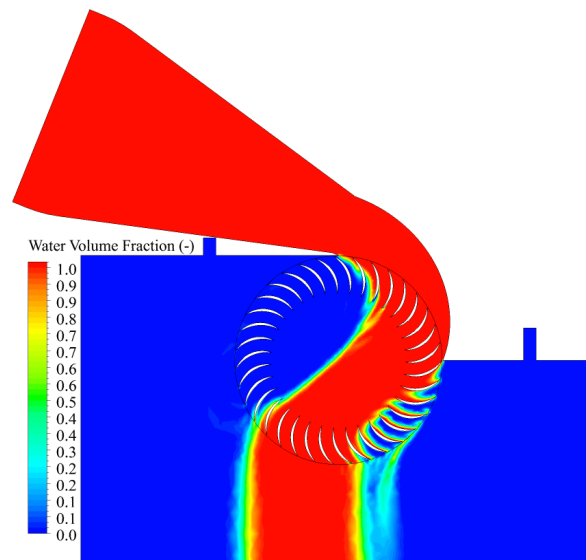
Figure 17. Pressure contours.
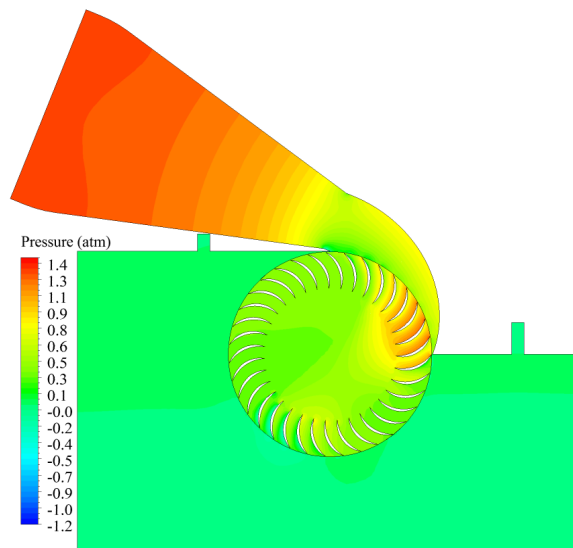
Figure 18. Water velocity field contours.
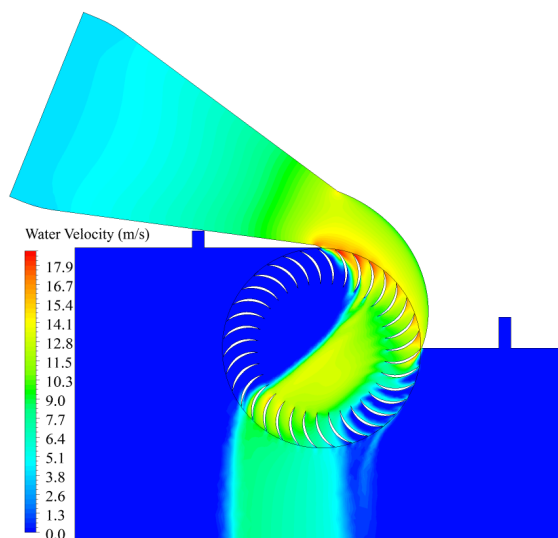
Finally, it should be observed that the relative pressure computed at the inlet of the nozzle was close to zero. This is consistent with the classification of "action turbine" given to the cross-flow machine and allows easy estimation of the turbine characteristic curve, where the upstream hydraulic head is mainly given by kinetic energy of the flow rate at the nozzle inlet.

The cross flow designed with this procedure has an impeller without the rotating shaft. To complete the bi-dimensional analysis it is important to test the effect of the rotating shaft on the efficiency of the turbine. Starting from the optimum geometry of the designed turbine, whose geometric parameters are reported in Table 4, an additional series of simulations were carried out considering an impeller with a rotating shaft of 20 mm diameter. The results of these simulations are summarized in the efficiency curve in Figure 19. In this figure the efficiencies of the turbine with and without the rotating shaft are compared. As shown in Figure 19, even if the trend of the curves is quite similar, the rotating shaft reduces the efficiency of the designed turbine. In particular, the reduction in efficiency increased as the water discharge increased; for the discharge project value (Q = 60 l/s) the efficiency reduction was about 4%.

Figure 19. Efficiency curves of the turbine with and without the rotating shaft.
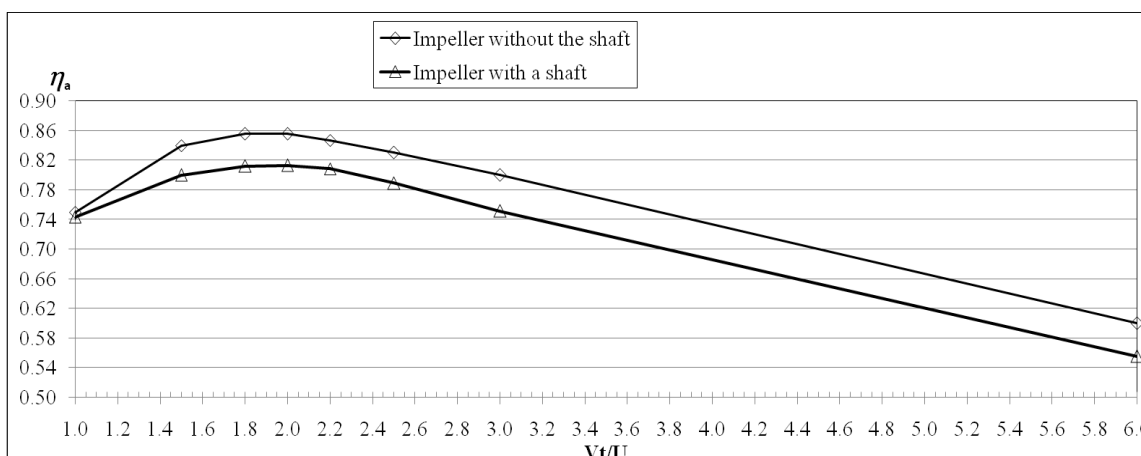
The characteristic curves on the plane *H-Q* are reported in Figure 20.They show that for the design value of water discharge (Q = 60 l/s) the turbine with and without a rotating shaft has the same value of upstream hydraulic head H = 14.2 m. The curves show a difference in the hydraulic head H in the two configurations for larger values of water discharge.

Figure 20. Characteristic curves on *H-Q* plane of the turbine with and without the shaft.
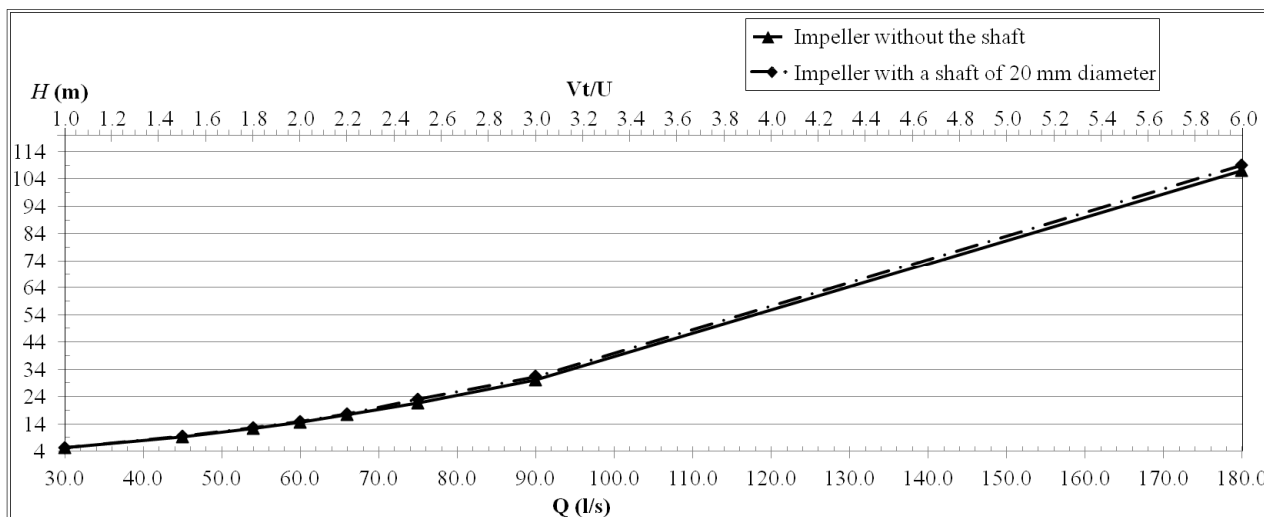
5.2. 3D-Simulations: Spread Ratio Tests

A second series of numerical simulations were carried out in order to test the effect of the flow stream spread W/B on the turbine performance, using a fully 3D numerical approach. The mesh and the boundary conditions used in these simulations are described in section 4. The instantaneous output power P_{out} calculated for two different ratios W/B, equal respectively to 1.5 and 1.0, are plotted in Figure 21 *versus* time. The resulting average efficiencies were respectively, 78% and 85%, while the respective power outputs were 4.73 KW and 5.03 KW. This result suggests that, at least in this particular case, the use of a larger stream spread W/B equal to 1.5 does not improve the efficiency of the turbine, in disagreement with the results of Aziz and Desai [10]. Indeed, when the nozzle has the same width as the impeller (W/B = 1) the average efficiency is 85%, against the 78% value obtained for W/B = 1.5. Also observe that the average efficiency obtained for the W/B = 1 value using a 3D approach is very close to the ratio computed using a more simple 2D approach. This validates the overall procedure, based on 2D computations.

Figure 21. The instantaneous values of the output power P_{out} of the turbine for two different values of the W/B ratio: W/B = 1.0 and W/B = 1.5.
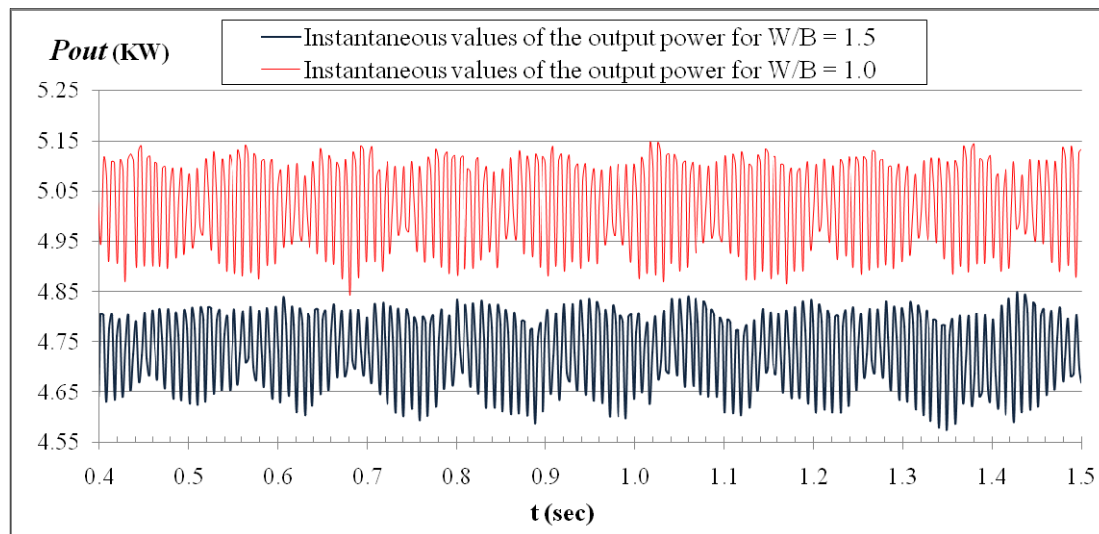
6. Conclusions

Banki-Michell turbines are a feasible choice for the exploitation of small hydropower sources because of their simplicity and their good efficiency, but a complete step-by-step procedure for their design was missing to the authors' knowledge. Starting from a theoretical study of the behavior of the machine, a two-step procedure has been proposed here. In the first step, some critical design parameters were theoretically estimated, on the basis of some simplifying assumptions. In the second step, the influence on the efficiency of the remaining design parameters was analyzed by means of CFD numerical testing. The new design procedure was applied to the development of a specific power plant, for a given design point, *i.e.*, the hydraulic head *H* and the water discharge *Q*. In this test case the turbine with 35 blades and an attack angle equal to 22° exhibited at the design point a high efficiency *η* equal to 86%. The 2D CFD analyses showed that the linear nozzle ensures an almost constant value of the angle of attack and confirms the simplifying hypothesis of negligible energy dissipation inside the impeller, which is a cornerstone of the theoretical approach. The number of blades and the diameter ratio has little influence on the peak efficiency, while the authors found that the presence of the shaft does not affect the characteristic curve, but leads to a considerable reduction in efficiency. The 3D simulations—carried out for the designed optimal configuration—suggest an optimal value of the ratio between the width of the impeller and of the nozzle equal to one; this validates the adopted 2D approach, but disagrees with previous literature results [10].

Acknowledgments

References

1. Anagnostopoulos, J.S.; Papantonis, D.E. Optimal sizing of a run-of-river small hydropower plant. *Energy Convers. Manag.* **2007**, *48*, 2663–2670.
2. Hosseinia, S.M.H.; Forouzbakhshb, F.; Rahimpoora, M. Determination of the optimal installation capacity of small hydro-power plants through the use of technical, economic and reliability indices. *Energy Policy* **2005**, *33*, 1948–1956.
3. Carravetta, A.; del Giudice, G.; Fecarotta, O.; Ramos, H. Energy production in water distribution networks: A PAT design strategy. *Water Resour. Manag.* **2012**, *26*, 3947–3959.
4. Carravetta, A.; del Giudice, G.; Fecarotta, O.; Ramos, H. PAT Design strategy for energy recovery in water distribution networks by electrical regulation. *Energies* **2013**, *6*, 411–424.
5. Chapallaz, J.M.; Eichenberger, P. Guida Pratica per la Realizzazione di Piccole Centrali Idrauliche [in Italian]; Ufficio federale dei problemi congiunturali: Berne, Switzerland, **1992**; ISBN 3-905232-20-0 (French ver.); ISBN 3-905232-38-3 (Italian ver.).
6. Penche, C. *Guide on How to Develop a Small Hydropower Plant*; European Small Hydropower Association: Brussels, Belgium, **2004**.
7. Khosrowpanah, S.; Albertson, M.L.; Fiuzat, A.A. Historical overview of cross-flow turbine. *Int. Water Power Dam Constr.* **1984**, *36*, 38–43.
8. Fiuzat, A.A.; Akerkar, B.P. The Use of Interior Guide Tube in Cross Flow Turbines. In Proceedings of the International Conference on Hydropower-WATERPPOWER '89, London, UK, 21–26 August **1989**.
9. Fiuzat, A.A.; Akerkar, B.P. Power outputs of two stages of cross-flow turbine. *J. Energy Eng.* **1991**, *117*, 57–70.
10. Aziz, N.M.; Desai, V.R. A Laboratory Study to Improve the Efficiency of Cross-Flow Turbines. In *Engineering Report*; Department of Civil Engineering, Clemson University, Clemson, SC, USA, **1993**.
11. De Andrade, J.; Curiel, C.; Kenyery, F.; Aguillón, O.; Vásquez, A.; Asuaje, M. Numerical investigation of the internal flow in a Banki turbine. *Int. J. Rotating Mach.* **2011**, 841214:1–841214:12.
12. Mockmore, C.A.; Merryfield, F. The Banki Water Turbine. In *Bullettin Series*, *Engineering Experiment Station*; Oregon State System of Higher Education, Oregon State College: Corvallis, OR, USA, **1949**.
13. Aziz, N.M.; Totapally, H.G.S. Design Parameter Refinement for Improved Cross-Flow Turbine Performance; In *Engineering Report*; Departement of Civil Engineering, Clemson University, Clemson, SC, USA, **1994**.
14. Choi, Y.; Lim, J.; Kim, Y.; Lee, Y. Performance and internal flow characteristics of a cross-flow hydro turbine by the shapes of nozzle and runner blade. *J. Fluid Sci. Technol.* **2008**, *3*, 398–409.
15. Hothersall, R.J. Micro hydro: Turbine selection criteria. *Int. Water Power Dam Constr.* **1984**, *36*, 26–29.
16. Khosrowpanah, S.; Fiuzat, A.A.; Albertson, M.L. Experimental study of cross-flow turbine. *J. Hydraul. Eng.* **1988**, *114*, 299–314.

17. Desai, V.R.; Aziz, N.M. An experimental investigation of cross-flow turbine efficiency. *J. Fluid Eng.* **1994**, *116*, 45–550.

18. Nakase, Y.; Fukatomi, J.; Watanaba, T.; Suetsugu, T.; Kubota, T.; Kushimoto, S. A Study of Cross-flow Turbine (Effects of Nozzle Shape on its Performance). In Proceedings of the Winter Annual Meeting A.S.M.E., Phoenix, AZ, USA, 14–19 November 1982; Webb, D.R., Papadakis, C., Eds.; In *Small Hydro Power Fluid Machinery*; American Society of Mechanical Engineers (ASME): New York, NY, USA, **1982**; pp. 13–18.

19. Ansys Inc. *ANSYS CFX Reference Guide*; Ansys Inc.: Canonsburg, PA, USA, **2006**.